Revisiting the structure of $[PdAu_9(PPh_3)_8(CN)]^{2+}$ produced by atmospheric pressure plasma irradiation of $[PdAu_8(PPh_3)_8]^{2+}$ in methanol

Takumi Imagawa,[1] Shun Ito,[1] Frank Hennrich,[2,3] Marco Neumaier,[2,4] Patrick Weis,[2] Kiichirou Koyasu,[1] Manfred M. Kappes,[2,3,4,a)] and Tatsuya Tsukuda[1,a)]

AFFILIATIONS

[1] Department of Chemistry, Graduate School of Science, The University of Tokyo, 7-3-1 Hongo, Bunkyo-ku, Tokyo 113-0033, Japan
[2] Institute of Physical Chemistry, Karlsruhe Institute of Technology, Fritz-Haber-Weg 2, 76131 Karlsruhe, Germany
[3] Institute of Quantum Materials and Technologies, Karlsruhe Institute of Technology, Hermann-von- Helmholtz-Platz 1, 76344 Eggenstein-Leopoldshafen, Germany
[4] Institute of Nanotechnology, Karlsruhe Institute of Technology, Hermann-von-Helmholtz-Platz 1, 76344 Eggenstein-Leopoldshafen, Germany

[a)] **Authors to whom correspondence should be addressed:** manfred.kappes@kit.edu and tsukuda@chem.s.u-tokyo.ac.jp

ABSTRACT

Some of the authors of the present research group have previously reported mass spectrometric detection of $[PdAu_9(PPh_3)_8(CN)]^{2+}$ (**$PdAu_9CN$**) by atmospheric pressure plasma (APP) irradiation of $[MAu_8(PPh_3)_8]^{2+}$ (**$PdAu_8$**) in methanol and proposed based on density functional theory (DFT) calculations that **$PdAu_9CN$** is constructed by inserting a CNAu or NCAu unit into the Au–PPh_3 bond of **$PdAu_8$** [Emori *et al.*, J. Chem. Phys. **155**, 124312 (2021)]. In this follow-up study, we revisited the structure of **$PdAu_9CN$** by high-resolution ion mobility spectrometry on an isolated sample of **$PdAu_9CN$** with the help of dispersion-corrected DFT calculation. In contradiction to the previous proposal, we conclude that isomers in which an AuCN unit is directly bonded to the central Pd atom of **$PdAu_8$** are better candidates. This assignment was supported by Fourier transform infrared and ultraviolet–visible spectroscopies of isolated **$PdAu_9CN$**. The simultaneous formation of $[Au(PPh_3)_2]^+$ and **$PdAu_9CN$** suggests that the AuCN species are formed by APP irradiation at the expense of a portion of **$PdAu_8$**. These results indicate that APP may offer a unique method for transforming metal clusters into novel ones by generating *in situ* active species that were not originally added to the solution.

I. INTRODUCTION

In recent years, ligand-protected metal clusters with atomically defined sizes and structures have been found to be promising functional nanoscale materials.[1–8] Conventionally, they are synthesized by chemical reduction of the corresponding metal–ligand complexes, followed by isolation. The main challenges of such synthesis methods are low yields and unpredictability of size, shape, and composition of the metal clusters obtained. Transformation of a predefined metal cluster to another cluster[9] is a promising approach to overcome such synthesis problems. Transformation of the sizes and structures of metal clusters has been induced by a variety of methods, such as ligand exchange,[10,11] metal exchange,[12,13] hydride adsorption,[14] intercluster reactions,[15] photoirradiation,[16] redox reactions,[17] and change in pH[18] and temperature.[19]

Exposure to atmospheric pressure plasma (APP), which is typically generated by electrical discharge in flowing helium and produces reactive chemical species and energetic electrons under ambient conditions, has attracted attention as a nonthermal source for preparation[20–23] and surface treatment of nanoparticles and nanostructures.[24,25] For example, APP irradiation of $Au_{25}(SR)_{18}$ created exposed Au sites that were catalytically active for CO oxidation.[25] These examples suggest that APP may be used to trigger selective cluster transformation. To gain insight into what types of reactions are induced by APP, we recently irradiated methanol solutions of $[Au_9(PPh_3)_8]^{3+}$ and $[MAu_8(PPh_3)_8]^{2+}$ [**MAu_8**, M = Pd

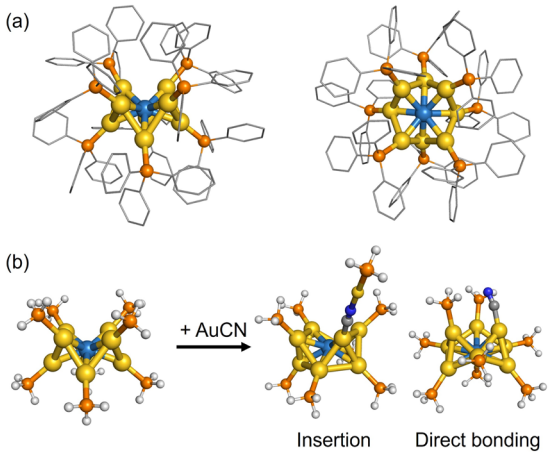

FIG. 1. (a) Side (left) and top (right) views of the structure of $[PdAu_8(PPh_3)_8]^{2+}$ having a crown-shaped Pd@Au_8 core. (b) DFT-optimized structures of $[PdAu_8(PH_3)_8]^{2+}$ and two isomers of $[PdAu_9(PH_3)_8(CN)]^{2+}$ as a model system of the APP-induced reaction of $[PdAu_8(PPh_3)_8]^{2+}$ in methanol.[26] Color code: Pd, cyan; Au, yellow; P, orange; H, white; C, gray; and N, blue.

and Pt, Fig. 1(a)] with APP and found that the following different transformations occurred, depending on the central atom:[26]

$$\left[PtAu_8(PPh_3)_8\right]^{2+} + CO \rightarrow \left[PtAu_8(PPh_3)_8(CO)\right]^{2+}, \quad (1)$$

$$\left[PdAu_8(PPh_3)_8\right]^{2+} + AuCN \rightarrow \left[PdAu_9(PPh_3)_8(CN)\right]^{2+}, \quad (2)$$

$$\left[Au_9(PPh_3)_8\right]^{3+} \xrightarrow{AuCN} \left[Au_x(PPh_3)_y(CN)_z\right]^{2+}, \quad (3)$$

where $(x, y, z) = (9, 7, 1)$, $(10, 8, 2)$, $(10, 7, 2)$, and $(11, 8, 3)$. Notably, clusters with unexpected compositions were obtained in Eqs. (2) and (3) by incorporating AuCN unit(s) generated by APP irradiation of the precursor clusters. Density functional theory (DFT) calculations (without dispersion correction) on simplified models of the products of Eqs. (2) and (3) predicted two bonding modes of AuCN to the precursors. Figure 1(b) exemplifies two such isomers of $[PdAu_9(PH_3)_8(CN)]^{2+}$.[26] One has a CNAu unit inserted into the Au–PH_3 bond to form a novel ligand $CNAuPH_3$ on the $PdAu_8$ core, while the other has an AuCN unit directly bonded to the $PdAu_8$ core to form a new $PdAu_9$ core with a $(-Au-Au_2-)_3$ ring motif. Based on these DFT calculations, the former structure type was tentatively assigned as a candidate structure for $[PdAu_9(PPh_3)_8(CN)]^{2+}$ (**$PdAu_9CN$**). However, no experimental evidence for the structure of the products has previously been provided because $[PdAu_9(PPh_3)_8(CN)]^{2+}$ could not be isolated.

In this follow-up study,[26] we successfully isolate **$PdAu_9CN$** and characterize its structure using ultraviolet–visible (UV–Vis) and Fourier transform infrared (FT-IR) spectroscopies, and high-resolution ion mobility spectrometry (IMS) in combination with DFT calculations including dispersion as well as ion trajectory simulations. In contradiction to the previous proposal,[26] we conclude that direct bonded isomers are better candidates for **$PdAu_9CN$**.

II. METHODS

A. Isolation and characterization of $[PdAu_9(PPh_3)_8(CN)]^{2+}$

Precursor cluster **$PdAu_8$** was synthesized according to reported procedures.[27] To prepare sufficient amounts of purified **$PdAu_9CN$** for structural characterization, we used a larger amount of **$PdAu_8$** than in the previous study (0.25 mg in 2 ml of methanol).[26] In particular, methanol solutions (2 ml) containing 0.25, 0.5, 1.0, or 2.0 mg of $[PdAu_8(PPh_3)_8](NO_3)_2$ were prepared in a 5 ml vial with a magnetic stirrer bar. The exit of the APP source (Fig. 2) was placed a few millimeters above the solution surface level, and the solution was APP-irradiated while being stirred gently. The APP setup and operation conditions are detailed in Ref. 26. During the irradiation, methanol was added to the solution to keep a sufficiently small distance between the APP source and the solution surface. After APP irradiation for a given period, the solution was evaporated to dryness and a brownish solid containing **$PdAu_9CN$** was obtained.

The collected sample of **$PdAu_9CN$** was characterized as follows: positive-mode electrospray ionization (ESI) mass spectra were recorded on a Bruker compact ESI-Q-TOF mass spectrometer. The isotope patterns were calculated using iMass software. UV–Vis absorption spectra were recorded on a Jasco V-630 spectrophotometer in the transmission mode using a 1 cm quartz cuvette.

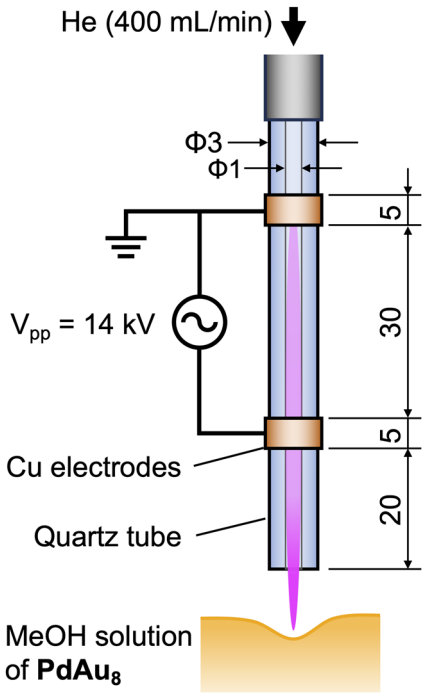

FIG. 2. Schematic diagram of the experimental setup. The numbers represent the dimensions in mm.

The absorbance was scaled by the Jacobian transformation when converting the abscissa values from wavelength to energy.[28] FT-IR spectroscopy was conducted using a Jasco FT/IR-4200 spectrophotometer. For this measurement, clusters were mixed with KBr, ground in an agate mortar, and compressed into a sample pellet. The experimental collision cross sections (CCS_{exp}) of isolated cationic clusters electrosprayed from solution were determined by traveling wave ion mobility measurement in nitrogen using a Waters Select Series Cyclic ion mobility mass (IMS) spectrometer[29,30] installed at Karlsruhe Institute of Technology. Measurement and CCS_{exp} calibration procedures are as described in Ref. 30. Absolute CCS_{exp} values given in this study are accurate to within 2% error. The (relative) precision, e.g., of the ratio of CCS_{exp} values for **$PdAu_8$** vs **$PdAu_9CN$** was significantly higher and in the order of 0.5%.

B. Theoretical calculations on $[PdAu_9(PPh_3)_8(CN)]^{2+}$

DFT calculations on **$PdAu_9CN$** were conducted using the Gaussian 16 program.[31] B3LYP was used as a functional, the LANL2DZ basis set was used for Pd and Au, and 6-31G(d) was used for P, C, N, and H. Stable structures of **$PdAu_9CN$** were obtained by optimizing the initial structures constructed according to the reported procedures[26] using the GaussView 6.1.1 software. Structural optimization was first conducted without dispersion correction, followed by inclusion of the D3 version of Grimme's dispersion with Becke–Johnson damping by adding the keyword "EmpiricalDispersion = GD3BJ." Finally, vibrational frequencies of the optimized structures were calculated to confirm that they had no imaginary frequencies and were located at the local minima of the potential energy surface. The electronic structures of the optimized structures were also calculated. The theoretical collision cross sections in nitrogen (CCS_{cal}) of the optimized structures were calculated by using the IMoS v1.09 program with the quadrupole interaction of N_2 with ions taken into account (assuming NBO partial charges on the ions).[32,33] As a reference, **$PdAu_8$** was structurally optimized at the same level of theory, starting from the crystal structure.[34] The electronic structure and CCS_{cal} value of **$PdAu_8$** were also calculated.

III. RESULTS AND DISCUSSION

A. Isolation and characterization of $[PdAu_9(PPh_3)_8(CN)]^{2+}$

The reaction induced by APP irradiation of the methanol solution of **$PdAu_8$** was monitored by optical spectroscopy and mass spectrometry. First, the effect of the initial concentration of **$PdAu_8$** on the reaction process was studied. Figure S1 shows the positive-mode ESI mass spectra of the methanol solutions containing various amounts of **$PdAu_8$** after APP irradiation times (T_P) of 4 and 8 min. With the increase in T_P, the peak intensities of **$PdAu_9CN$** and $[Au(PPh_3)_2]^+$ increased, while that of **$PdAu_8$** decreased, as reported previously.[26] These results suggest that the chemical processes were not significantly affected by the concentration of **$PdAu_8$**. However, the percentage conversion (for a given irradiation time) was reduced with an increase in the concentration of **$PdAu_8$**. This trend was also confirmed by optical spectroscopy, as shown in Fig. S2.

Next, we attempted to determine the minimal T_P value required for full conversion of **$PdAu_8$** with the highest concentration in methanol (2 mg/2 ml) to **$PdAu_9CN$**. The ESI mass spectra of the irradiated solution in Fig. 3(a) show that the peak intensity of **$PdAu_8$** gradually decreased with T_P and diminished at T_P = 32 min, while those of **$PdAu_9CN$** and $[Au(PPh_3)_2]^+$ increased with T_P. This result indicates that the conversion of **$PdAu_8$** to **$PdAu_9CN$** was completed at T_P = 32 min. Peak δ in Fig. 3(a) tentatively assigned to $[Au_3(PPh_3)_3S]^+$ (Fig. S3) was newly observed compared with the previous report[26] due to the contamination of the mass spectrometer. Nevertheless, this species did not affect the characterization results of **$PdAu_9CN$**, because it was not produced in the sample but formed in the mass spectrometer. Figure 3(b) shows the UV–Vis spectra as a function of T_P. At T_P = 16 min, the characteristic peaks of **$PdAu_8$** at ~4 and 3.0 eV and a hump at ~2.4 eV [indicated by triangles in Fig. 3(b)] almost disappear, while the two peaks at 2.7 and 3.6 eV remain. The spectral profiles at T_P = 24 and 32 min are very similar, indicating that **$PdAu_8$** was completely transformed at T_P = 32 min to **$PdAu_9CN$** that was robust to APP exposure.

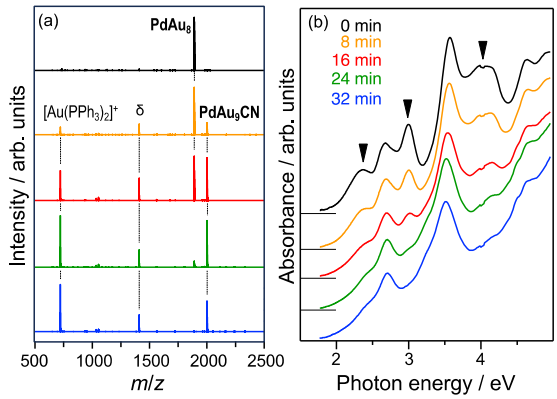

FIG. 3. (a) Positive-mode ESI mass spectra and (b) UV–Vis absorption spectra of the methanol solution of **$PdAu_8$** (1 mg/ml) after APP irradiation for T_P = 0 (black), 8 (orange), 16 (red), 24 (green), and 32 min (blue). The characteristic peaks of **$PdAu_8$** are indicated by triangles in panel (b).

Then, **$PdAu_9CN$** was isolated from the crude product obtained at T_P = 32 min as follows. The crude product was dissolved in a small amount of dichloromethane, and the solution was added dropwise to diisopropyl ether. The formed precipitate was separated from the supernatant after centrifugation and dried *in vacuo*. Positive-mode ESI mass spectrometry of the purified samples confirmed the removal of $[Au(PPh_3)_2]^+$. By repeating the same procedure with the precipitates, by-products were further removed, and finally, **$PdAu_9CN$** was obtained in purified form (Fig. S4). Figure 4 shows the positive-mode ESI mass spectrum and UV–Vis absorption spectrum of the purified **$PdAu_9CN$**. The experimental isotope pattern of the purified **$PdAu_9CN$** was in good agreement with the simulated one, indicating that the cluster composition remained unchanged during the reprecipitation. Absorption bands of the purified **$PdAu_9CN$** at 3.5 and 4.6 eV became more prominent due to the removal of $[Au(PPh_3)_2]^+$. The optical gap was determined from the spectral onset to be 1.9 ± 0.2 eV, which is comparable to that of **$PdAu_8$** (1.95 eV).[35]

Figure 5 shows the mobilograms (i.e., ion intensity vs collision cross section) for **$PdAu_8$** and **$PdAu_9CN$**. These were obtained

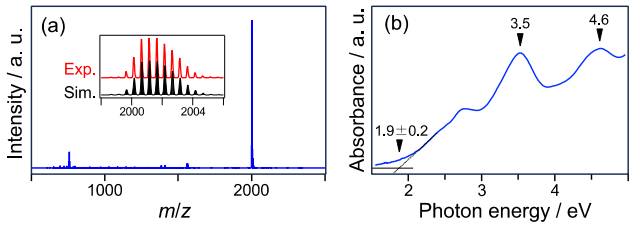

FIG. 4. (a) Positive-mode ESI mass spectrum and (b) UV–Vis absorption spectrum of purified **PdAu$_9$CN**. The inset in panel (a) is a comparison of the experimental and simulated isotope patterns of **PdAu$_9$CN**.

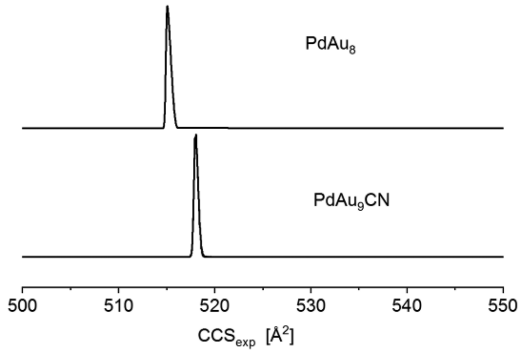

FIG. 5. High resolution (130 cycles) mobilograms for **PdAu$_8$** and **PdAu$_9$CN** as determined with a Waters Select Series Cyclic ion mobility mass spectrometer. CCS$_{exp}$ values were 515 and 518 Å^2, respectively.

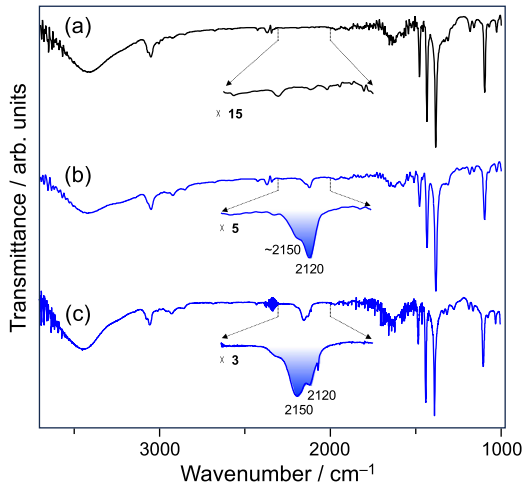

FIG. 6. FT-IR spectra of (a) **PdAu$_8$** and (b) and (c) two independent batches of purified **PdAu$_9$CN**.

from the respective ion arrival time distributions (ATDs) measured under identical conditions for both clusters (TW height 22 V, speed 375 m/s, and 130 cycles). The conversion procedure from ATD to calibrated mobilogram is described in Ref. 30. The mobilograms show one maximum, each suggesting the presence of only a single isomer. The corresponding CCS$_{exp}$ values of **PdAu$_8$** and **PdAu$_9$CN** were determined to be 515 and 518 Å^2 with an error of 10 Å^2. The similar CCS$_{exp}$ values for **PdAu$_8$** and **PdAu$_9$CN** show that **PdAu$_9$CN** retains the structural bulkiness of **PdAu$_8$** despite the addition of an AuCN unit.

Figure 6 shows the FT-IR spectra of **PdAu$_8$** and **PdAu$_9$CN**. The spectrum of **PdAu$_9$CN** shows a peak at 2120 cm^{-1} with a shoulder at 2150 cm^{-1} [Fig. 6(b)], while that of **PdAu$_8$** does not [Fig. 6(a)]. These peaks can be assigned to the stretching mode of a C≡N bond typically observed in the range of 2000–2200 cm^{-1}. This result is direct evidence of the presence of a C≡N moiety in **PdAu$_9$CN**. Furthermore, the relative intensity of the two peaks changes depending on the batch of samples [Figs. 6(b) and 6(c)]. This result implies the existence of structural isomers in **PdAu$_9$CN**.

B. DFT calculations on [PdAu$_9$(PPh$_3$)$_8$(CN)]$^{2+}$

To gain structural insight into **PdAu$_9$CN**, we previously conducted DFT calculations on the simplified model system [PdAu$_9$(PH$_3$)$_8$(CN)]$^{2+}$ and obtained two isomeric structures, as shown in Fig. 1(b).[26] In the present study, more extensive DFT calculations were conducted: (1) the authentic PPh$_3$ ligand was used instead of PH$_3$; (2) more initial structures were surveyed for structural optimization; (3) dispersion correction was included for a better description of electronic and geometric structures;[30] and (4) the CCS value, C≡N stretching frequencies, and optical gap were calculated for each isomer for comparison with the experimental results.

Five initial structures **a**–**e** were prepared for energy optimization as follows: structures **a** and **b** were constructed by inserting a CNAu or NCAu unit into the Au–PPh$_3$ bond of **PdAu$_8$**, respectively. The other three structures **c**–**e** were constructed by coordinating an AuCN unit to the central Pd atom of **PdAu$_8$**. In structures **c** and **d**, the CN ligand was bonded to an Au$_2$ or Au site of the outer ring (–Au–Au$_2$–)$_3$ of an oblate PdAu$_9$ core, respectively. In structure **e**, the CN was bonded to an Au atom located on the C_3 axis of the PdAu$_9$ core. Table I summarizes the optimized structures **A**–**E** obtained from **a**–**e**, respectively. The analysis of vibrational frequencies indicated that all the isomers corresponded to local minimum structures. Isomers **A** and **C** corresponded to the structures reported previously [Fig. 1(b)],[26] whereas isomers **B**, **D**, and **E** were newly obtained in the present work. In sharp contrast to the previous DFT results obtained without dispersion corrections,[26] isomers **C**–**E** were more stable than **A** and **B** by about 1 eV.

Table I lists the CCS$_{cal}$ values of each isomer. The CCS$_{cal}$ value of **PdAu$_8$** was 537.0 Å^2, which is comparable to those of isomers **C**–**E**, but significantly smaller than those of **A** and **B**. Since the CCS$_{exp}$ values for **PdAu$_9$CN** and **PdAu$_8$** were comparable, the qualitative trend in CCS$_{cal}$ values clearly indicates that isomers **C**–**E** are more probable candidates for **PdAu$_9$CN**. The calculated frequencies of the C≡N stretching mode are also listed in Table I. The calculated values were scaled by a factor of 0.952 using the C≡N stretching frequency of CH$_3$CN experimentally observed (2268 cm^{-1})[36] and that theoretically predicted at the same level of calculation (2381.75 cm^{-1}). The experimental vibrational frequencies (2120 and 2150 cm^{-1}, Fig. 6) are explained by **C**, **D**, or **E**, although a contribution from **A** and/or **B** cannot be excluded completely.

TABLE I. Summary of optimized structures of **$PdAu_9CN$**.[a]

Isomer	A	B	C	D	E
Optimized structures[a]	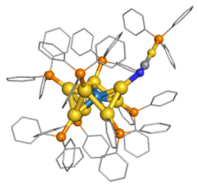	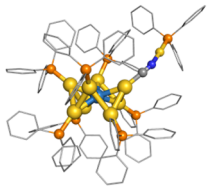	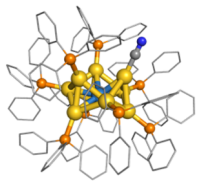	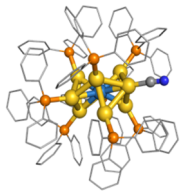	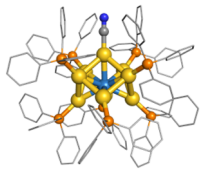
ΔE (eV)[b]	1.21	1.29	0	0.26	0.20
CCS_{cal} (Å^2)[c]	566	568	527	533	540
ν_{CN} (cm^{-1})[d]	2132	2107	2134	2130	2141
ΔE_{HL+1} (eV)[e]	2.95	2.94	3.09	3.01	2.93

[a]Color code: Pd, cyan; Au, yellow; P, orange; C, gray; and N, blue.
[b]Relative energy with zero-point energy.
[c]Experimental collision cross section, CCS_{exp} = 518 Å^2.
[d]Frequencies of C≡N stretching mode obtained by multiplying the calculated values by a scaling factor of 0.952, which was derived from the ratio of experimental to theoretical stretching mode of CH_3CN (Ref. 35). Experimental frequencies = 2120 and 2150 cm^{-1}.
[e]Energy gap between HOMO and LUMO+1. Experimental optical gap = 1.9 ± 0.2 eV.

The energy levels of the Kohn–Sham (KS) orbitals of isomers **A**–**E** are shown in Fig. 7. The shapes of the KS orbitals shown in Fig. S5 indicate that the highest occupied molecular orbital (HOMO), HOMO-1, and the lowest unoccupied molecular orbital (LUMO) of **A**–**E** correspond to the superatomic 1P orbitals. The splitting of three 1P orbitals into two sub-groups is associated with the oblate shape of the $PdAu_8$ cores in **A** and **B** and the $PdAu_9$ cores in **C**–**E**. One of the 1P orbitals along the compressed direction becomes destabilized compared with the other two 1P orbitals to form the LUMO. As a result, isomers **A**–**E** take the subshell-closed electron configuration of $(1S)^2(1P)^4$. A similar electronic structure was also observed in the precursor **$PdAu_8$** (Figs. 7 and S5). Nevertheless, close inspection of Fig. 7 reveals that the KS orbitals of **C**–**E** are significantly more stable than those of **$PdAu_8$**, while those of **A** and **B** are close in energy to those of **$PdAu_8$**. This trend can be explained in terms of the larger core volume of **C**–**E** for electron confinement than that of **$PdAu_8$**. The electronic transition from HOMO to LUMO is optically forbidden because they both have 1P characteristics. Thus, the minimum energy optical transition occurred from HOMO to LUMO + 1. The energy gap between HOMO and LUMO + 1 (ΔE_{HL+1}) was calculated for each isomer and is listed in Table I. The calculated ΔE_{HL+1} values for isomers **A**–**E** (~3 eV) are significantly larger than the experimental optical onset of **$PdAu_9CN$** [1.9 ± 0.2 eV, Fig. 4(b)] and differ by no more than 0.2 eV at most. Thus, unfortunately, it is not possible to narrow down the list of candidates based on the optical gap. Nevertheless, the experimental result that the optical gap is almost the same for **$PdAu_9CN$** and **$PdAu_8$** [Fig. 4(b)] was reproduced in the DFT calculation (Table I).

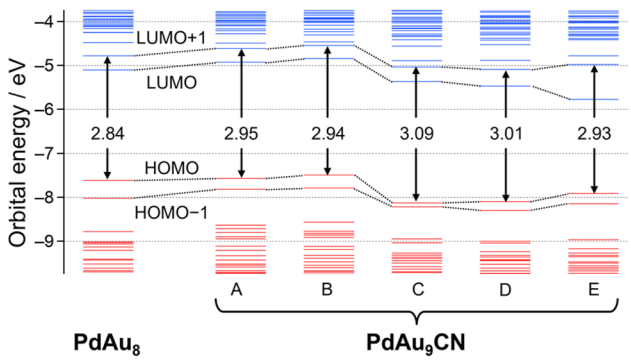

FIG. 7. Electronic structures of optimized structure of **$PdAu_8$** and isomers **A–E** of **$PdAu_9CN$**. The calculated ΔE_{HL+1} values are also given.

In contradiction to the previous suggestion,[26] we concluded from the IMS measurements and CCS_{cal} simulations that isomers **C**–**E** are significantly better candidates for **$PdAu_9CN$** than isomers **A** and **B**. This assignment is also consistent with the DFT-based energetic ordering predicted after taking the dispersion correction into account: isomers **A** and **B** are less stable than **C**–**E** by about 1 eV. It should be noted that the formation of isomers **A** and **B** is kinetically unfavorable because it would require surmounting a high energy barrier for the insertion of AuCN into the Au–PPh_3 bond. Such a prohibitive kinetic barrier for bond insertion is also supported by the absence of products in which more than one AuCN unit is incorporated into **$PdAu_8$**. The FT-IR and optical spectroscopic results are consistent with the formation of **C**–**E**, although they do not help further narrow down the candidates. The simultaneous formation of $[Au(PPh_3)_2]^+$ and **$PdAu_9CN$** suggests that the AuCN species are formed by APP irradiation at the expense of a portion of **$PdAu_8$**. Then, how was the AuCN species formed? It was reported that active nitrogen, such as N atoms and electronically excited N_2^* produced by electrical discharge, generates HCN through the reaction with CH_3OH.[37] We proposed that similar processes are involved in the formation of AuCN based on our previous observation of the emission lines of N_2^* and N_2^+ from the He APP.[26] Although further studies are necessary to elucidate the

detailed mechanism, the current results indicate that APP may offer a unique opportunity to transform metal clusters into novel ones by generating *in situ* active species that were not originally present in the solution.

IV. SUMMARY

In summary, $[PdAu_9(PPh_3)_8(CN)]^{2+}$ (**$PdAu_9CN$**) selectively obtained from $[MAu_8(PPh_3)_8]^{2+}$ (**$PdAu_8$**) by atmospheric pressure plasma (APP) irradiation was isolated by fractional precipitation. High-resolution ion mobility spectrometry of **$PdAu_9CN$** revealed that the collision cross section (CCS) is comparable to the **$PdAu_8$** precursor. Density functional theory (DFT) calculations with dispersion correction show that direct binding of an AuCN unit to the central Pd atom of **$PdAu_8$** hardly changes the CCS value, whereas insertion of a CNAu or NCAu unit into the Au–PPh_3 bond of **$PdAu_8$** significantly i ncreases i t. D FT c alculations a lso p redict t hat the former type of isomers having $PdAu_9$ cores is more stable than the latter type of isomers retaining $PdAu_8$ cores by ~1 eV. These results indicate that **$PdAu_9CN$** comprises a $PdAu_9$ core in contrast to the tentative structural inference in a previous study.[26] The FT-IR and optical spectroscopic results are consistent with this assignment.

ACKNOWLEDGMENTS

This research was financially supported by JST, CREST (Grant No. JPMJCR20B2), and JSPS KAKENHI (Grant Nos. JP20H00370 and JP21J20631). M.M.K. and P.W. acknowledge the support by Karlsruhe Institute of Technology (KIT) and DFG (Grant No. CRC 1578).

AUTHOR DECLARATIONS

Conflict of Interest

The authors have no conflicts to disclose.

Author Contributions

Takumi Imagawa: Data curation (lead); Formal analysis (equal); Investigation (equal). **Shun Ito**: Data curation (supporting); Formal analysis (supporting); Investigation (equal). **Frank Hennrich**: Data curation (equal); Formal analysis (equal); Investigation (equal). **Marco Neumaier**: Data curation (equal); Formal analysis (equal); Investigation (equal). **Patrick Weis**: Data curation (equal); Formal analysis (equal); Investigation (equal). **Kiichirou Koyasu**: Data curation (equal); Formal analysis (equal); Investigation (equal). **Manfred M. Kappes**: Data curation (equal); Methodology (equal); Supervision (equal); Writing – review & editing (equal). **Tatsuya Tsukuda**: Conceptualization (equal); Funding acquisition (equal); Supervision (equal); Writing – original draft (equal); Writing – review & editing (equal).

DATA AVAILABILITY

The data that support the findings of this study are available from the corresponding author upon reasonable request.

REFERENCES

[1] R. Jin, C. Zeng, M. Zhou, and Y. Chen, Chem. Rev. **116**, 10346 (2016).
[2] I. Chakraborty and T. Pradeep, Chem. Rev. **117**, 8208 (2017).
[3] Y. Du, H. Sheng, D. Astruc, and M. Zhu, Chem. Rev. **120**, 526 (2020).
[4] X. Kang, Y. Li, M. Zhu, and R. Jin, Chem. Soc. Rev. **49**, 6443 (2020).
[5] S. Takano and T. Tsukuda, J. Am. Chem. Soc. **143**, 1683 (2021).
[6] M. F. Matus and H. Häkkinen, Nat. Rev. Mater. **8**, 372 (2023).
[7] S. Hossain, D. Hirayama, A. Ikeda, M. Ishimi, S. Funaki, A. Samanta, T. Kawawaki, and Y. Negishi, Aggregate **4**, e255 (2023).
[8] E. L. Albright, T. I. Levchenko, V. K. Kulkarni, A. I. Sullivan, J. F. DeJesus, S. Malola, S. Takano, M. Nambo, K. Stamplecoskie, H. Häkkinen, T. Tsukuda, and C. M. Crudden, J. Am. Chem. Soc. **146**, 5759 (2024).
[9] X. Zou, X. Kang, and M. Zhu, Chem. Soc. Rev. **52**, 5892 (2023).
[10] C. Zeng, Y. Chen, A. Das, and R. Jin, J. Phys. Chem. Lett. **6**, 2976 (2015).
[11] X. Yuan, X. Dou, K. Zheng, and J. Xie, Part. Part. Syst. Charact. **32**, 613 (2015).
[12] Z. Gan, N. Xia, and Z. Wu, Acc. Chem. Res. **51**, 2774 (2018).
[13] S. Wang, Q. Li, X. Kang, and M. Zhu, Acc. Chem. Res. **51**, 2784 (2018).
[14] S. Takano, S. Hasegawa, M. Suyama, and T. Tsukuda, Acc. Chem. Res. **51**, 3074 (2018).
[15] K. R. Krishnadas, A. Ghosh, A. Baksi, I. Chakraborty, G. Natarajan, and T. Pradeep, J. Am. Chem. Soc. **138**, 140 (2016).
[16] C. Tominaga, H. Hasegawa, K. Yamashita, R. Arakawa, and H. Kawasaki, RSC Adv. **6**, 73600 (2016).
[17] T. Higaki, C. Liu, Y. Chen, S. Zhao, C. Zeng, R. Jin, S. Wang, N. L. Rosi, and R. Jin, J. Phys. Chem. Lett. **8**, 866 (2017).
[18] Y. Yu, X. Chen, Q. Yao, Y. Yu, N. Yan, and J. Xie, Chem. Mater. **25**, 946 (2013).
[19] S. Gratious, S. Mukherjee, and S. Mandal, J. Phys. Chem. Lett. **13**, 9014 (2022).
[20] P. Maguire, D. Rutherford, M. Macias-Montero, C. Mahony, C. Kelsey, M. Tweedie, F. Peŕez-Martin, H. McQuaid, D. Diver, and D. Mariotti, Nano Lett. **17**, 1336 (2017).
[21] D. Sun, J. McLaughlan, L. Zhang, B. G. Falzon, D. Mariotti, P. Maguire, and D. Sun, Langmuir **35**, 4577 (2019).
[22] H.-T. Chen, D. Lee, and S. Linic, Chem. Mater. **35**, 6557 (2023).
[23] C. Xu, S. Chaudhuri, J. Held, H. P. Andaraarachchi, G. C. Schatz, and U. R. Kortshagen, J. Phys. Chem. Lett. **14**, 9960 (2023).
[24] J. H. M. Maurer, L. González-García, B. Reiser, I. Kanelidis, and T. Kraus, ACS Appl. Mater. Interfaces **7**, 7838 (2015).
[25] Y. Tan, H. Liu, X. Y. Liu, A. Wang, C. Liu, and T. Zhang, Chin. J. Catal. **39**, 929 (2018).
[26] S. Emori, S. Takano, K. Koyasu, and T. Tsukuda, J. Chem. Phys. **155**, 124312 (2021).
[27] S. Takano, H. Hirai, S. Muramatsu, and T. Tsukuda, J. Am. Chem. Soc. **140**, 12314 (2018).
[28] J. Mooney and P. Kambhampati, J. Phys. Chem. Lett. **4**, 3316 (2013).
[29] K. Giles, J. Ujma, J. Wildgoose, S. Pringle, K. Richardson, D. Langridge, and M. Green, Anal. Chem. **91**, 8564 (2019).
[30] F. Hennrich, S. Ito, P. Weis, M. Neumaier, S. Takano, T. Tsukuda, and M. M. Kappes, Phys. Chem. Chem. Phys. **26**, 8408 (2024).
[31] M. J. Frisch, G. W. Trucks, H. B. Schlegel, G. E. Scuseria, M. A. Robb, J. R. Cheeseman, G. Scalmani, V. Barone, G. A. Petersson, H. Nakatsuji, X. Li, M. Caricato, A. V. Marenich, J. Bloino, B. G. Janesko, R. Gomperts, B. Mennucci, H. P. Hratchian, J. V. Ortiz, A. F. Izmaylov, J. L. Sonnenberg, D. Williams-Young, F. Ding, F. Lipparini, F. Egidi, J. Goings, B. Peng, A. Petrone, T. Henderson, D. Ranasinghe, V. G. Zakrzewski, J. Gao, N. Rega, G. Zheng, W. Liang, M. Hada, M. Ehara, K. Toyota, R. Fukuda, J. Hasegawa, M. Ishida, T. Nakajima, Y. Honda,

O. Kitao, H. Nakai, T. Vreven, K. Throssell, J. A. Montgomery, Jr., J. E. Peralta, F. Ogliaro, M. J. Bearpark, J. J. Heyd, E. N. Brothers, K. N. Kudin, V. N. Staroverov, T. A. Keith, R. Kobayashi, J. Normand, K. Raghavachari, A. P. Rendell, J. C. Burant, S. S. Iyengar, J. Tomasi, M. Cossi, J. M. Millam, M. Klene, C. Adamo, R. Cammi, J. W. Ochterski, R. L. Martin, K. Morokuma, O. Farkas, J. B. Foresman, and D. J. Fox, Gaussian 16, Revision B.01, Gaussian, Inc., Wallingford, CT, 2016.

[32] C. Larriba-Andaluz and C. J. Hogan, J. Comput. Phys. **251**, 344 (2013).

[33] C. Larriba-Andaluz and C. J. Hogan, J. Chem. Phys. **141**, 194107 (2014).

[34] L. N. Ito, B. J. Johnson, A. M. Mueting, and L. H. Pignolet, Inorg. Chem. **28**, 2026 (1989).

[35] S. Matsuo, S. Takano, S. Yamazoe, K. Koyasu, and T. Tsukuda, ChemElectroChem **3**, 1206 (2016).

[36] E. L. Pace and L. J. Noe, J. Chem. Phys. **49**, 5317 (1968).

[37] M. J. Sole and P. A. Gartaganis, Can. J. Chem. **41**, 1097 (1963).